The Journal of Experimental Biology 205, 2413–2427 (2002)
Printed in Great Britain © The Company of Biologists Limited 2002
JEB4116

Lift and power requirements of hovering flight in *Drosophila virilis*

Mao Sun* and Jian Tang

Institute of Fluid Mechanics, Beijing University of Aeronautics and Astronautics, Beijing 100083, People's Republic of China

*e-mail: sunmao@public.fhnet.cn.net

Accepted 22 May 2002

Summary

The lift and power requirements for hovering flight in *Drosophila virilis* were studied using the method of computational fluid dynamics. The Navier–Stokes equations were solved numerically. The solution provided the flow velocity and pressure fields, from which the unsteady aerodynamic forces and moments were obtained. The inertial torques due to the acceleration of the wing mass were computed analytically. On the basis of the aerodynamic forces and moments and the inertial torques, the lift and power requirements for hovering flight were obtained.

For the fruit fly *Drosophila virilis* in hovering flight (with symmetrical rotation), a midstroke angle of attack of approximately 37 ° was needed for the mean lift to balance the insect weight, which agreed with observations. The mean drag on the wings over an up- or downstroke was approximately 1.27 times the mean lift or insect weight (i.e. the wings of this tiny insect must overcome a drag that is approximately 27 % larger than its weight to produce a lift equal to its weight). The body-mass-specific power was 28.7 W kg^{-1}, the muscle-mass-specific power was 95.7 W kg^{-1} and the muscle efficiency was 17 %.

With advanced rotation, larger lift was produced than with symmetrical rotation, but it was more energy-demanding, i.e. the power required per unit lift was much larger. With delayed rotation, much less lift was produced than with symmetrical rotation at almost the same power expenditure; again, the power required per unit lift was much larger. On the basis of the calculated results for power expenditure, symmetrical rotation should be used for balanced, long-duration flight and advanced rotation and delayed rotation should be used for flight control and manoeuvring. This agrees with observations.

Key words: fruit fly, *Drosophila virilis*, lift, power, unsteady aerodynamics, computational fluid dynamics.

Introduction

The lift and power requirements of hovering flight in insects were systematically studied by Weis-Fogh (1972, 1973) and Ellington (1984c) using methods based on steady-state aerodynamic theory. It was shown that the steady-state mechanism was inadequate to predict accurately the lift and power requirements of small insects and of some large ones (Ellington, 1984c).

In the past few years, much progress has been made in revealing the unsteady high-lift mechanisms of insect flight. Dickinson and Götz (1993) measured the aerodynamic forces on an aerofoil started impulsively at a high angle of attack [in the Reynolds number (*Re*) range of a fruit fly wing, *Re*=75–225] and showed that lift was enhanced by the presence of a dynamic stall vortex, or leading-edge vortex (LEV). Lift enhancement was limited to only 2–3 chord lengths of travel because of the shedding of the LEV. For most insects, a wing section at a distance of 0.5*R* (where *R* is wing length) from the wing base travels approximately 3.5 chord lengths during an up- or downstroke in hovering flight (Ellington, 1984b). A section in the outer part of the same wing travels a larger distance, e.g. a section at 0.75*R* from the wing base travels approximately 5.25 chord lengths, which is much greater than 2–3 chord lengths (in forward flight, the section would travel an even larger distance during a downstroke).

Ellington et al. (1996) performed flow-visualization studies on a hawkmoth *Manduca sexta* during tethered forward flight (forward speed in the range 0.4–5.7 m s^{-1}) and on a mechanical model of the hawkmoth wings that mimicked the wing movements of a hovering *Manduca sexta* [*Re*≈3500; in the present paper, *Re* for an insect wing is based on the mean velocity at r_2 (the radius of the second moment of wing area) and the mean chord length of the wing]. They discovered that the LEV on the wing did not shed during the translational motion of the wing in either the up- or downstroke and that there was a strong spanwise flow in the LEV. (They attributed the stabilization of the LEV to the effect of the spanwise flow.) The authors suggested that this was a new mechanism of lift enhancement, prolonging the benefit of the delayed stall for the entire stroke. Recently, Birch and Dickinson (2001) measured the flow field of a model fruit fly wing in flapping motion, which had a much smaller Reynolds number (*Re*≈70). They

also showed that the LEV did not shed during the translatory phase of an up- or downstroke.

Dickinson et al. (1999) conducted force measurements on flapping robotic fruit fly wings and showed that, in the case of advanced rotation, in addition to the large lift force during the translatory phase of a stroke, large lift peaks occurred at the beginning and near the end of the stroke. (In the case of symmetrical rotation, the lift peak at the beginning became smaller and was followed by a dip, and the lift peak at the end of the stroke also became smaller; in the case of delayed rotation, no lift peak appeared and a large dip occurred at the beginning of the stroke.) Recently, Sun and Tang (2002) simulated the flow around a model fruit fly wing using the method of computational fluid dynamics and confirmed the results of Dickinson et al. (1999). Using simultaneously obtained forces and flow structures, they showed that, in the case of advanced rotation, the large lift peak at the beginning of the stroke was due to the fast acceleration of the wing and that the large lift peak near the end of the stroke was due to the fast pitching-up rotation of the wing. They also explained the behaviour of forces in the cases of symmetrical and delayed rotation. As a result of these studies (Dickinson and Götz, 1993; Ellington et al., 1996; Dickinson et al., 1999; Birch and Dickinson, 2001; Sun and Tang, 2002), we are better able to understand how the fruit fly produces large lift forces. Although the above results were mainly derived from studies on fruit flies, it is quite possible that they are applicable to other insects that employ similar kinematics.

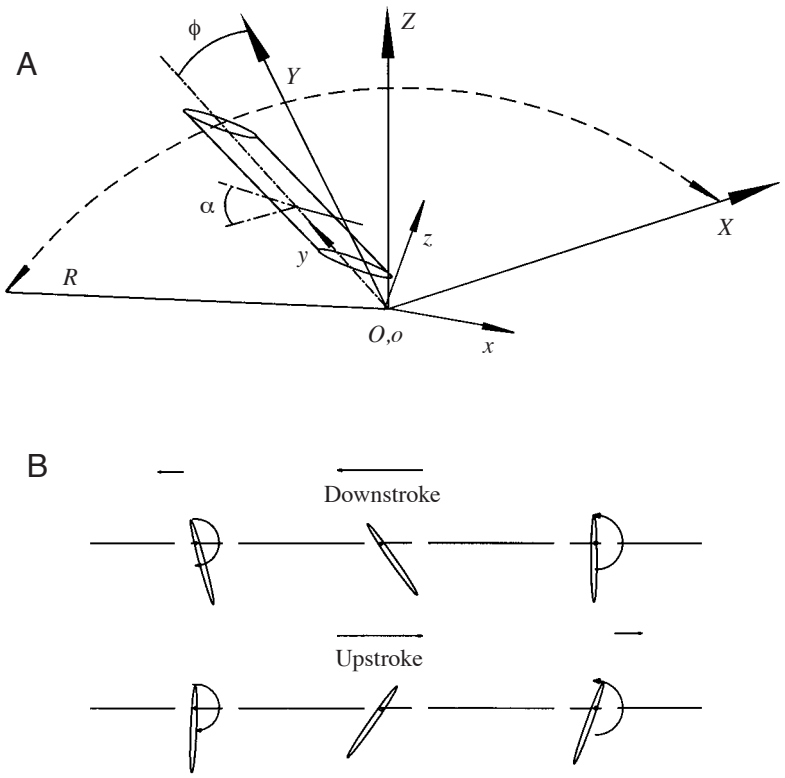

Fig. 1. Sketches of the reference frames and wing motion. (A) *OXYZ* is an inertial frame, with the *XY* plane in the stroke plane. *oxyz* is a frame fixed on the wing, with the *x* axis along the wing chord, and the *y* axis along the wing span. ϕ is the azimuthal angle of the wing, α is the angle of attack and *R* is the wing length. (B) The motion of a section of the wing.

The power requirements for generating lift through the unsteady mechanisms described above cannot be calculated using methods based on steady-state theory. In the rapid acceleration and fast pitching-up rotation mechanisms, virtual-mass force and force due to the generation of the 'starting' vortex exist, and they cannot be included in the power calculation using steady-state theory. In the delayed stall mechanism, the dynamic-stall vortex is carried by the wing in its translation, and the drag of the wing, and hence the power required, must be different from that estimated using steady-state theory. It is of great interest to determine the power required for generating lift through the unsteady mechanisms described above. Moreover, when the wing generates a large lift force through these unsteady mechanisms, a large drag force is also generated. For the fruit fly wing, the drag is significantly larger than the lift, as can be seen from the experimental data (Dickinson et al., 1999; Sane and Dickinson, 2001) and the computational results (Sun and Tang, 2002). From the computational results of Sun and Tang (2002), it is estimated that the mean drag coefficient over an up- or downstroke is more than 35 % greater than the mean lift coefficient. It is, therefore, of interest to determine whether these unsteady lift mechanisms are realistic from the energetics point of view.

Here, we investigate these problems for hovering flight in *Drosophila virilis* using computational fluid dynamics. In this method, the pressure and velocity fields around the flapping wing are obtained by solving the Navier–Stokes equations numerically, and the lift and torques due to the aerodynamic forces are calculated on the basis of the flow pressure and velocities. The inertial torques due to the acceleration and rotation of the wing mass can be calculated analytically. The mechanical power required for the flight may be calculated from the aerodynamic and inertial torques. The motion of the flapping wing and the reference frames are illustrated in Fig. 1.

Materials and methods

The wing and its kinematics

The wing considered in the present study is the same as that used in our previous work on the unsteady lift mechanism (Sun and Tang, 2002). The planform of the wing is similar to that of a fruit fly wing (see Fig. 2). The wing section is an ellipse of 12 % thickness (the radius of the leading and trailing edges is 0.2 % of the chord length of the aerofoil). The azimuthal rotation of the wing about the *Z* axis (see Fig. 1A) is called translation, and the pitching rotation of the wing near the end of a stroke and at the beginning of the following stroke is called

rotation or flip. The speed at the span location r_2 is called the translational speed of the wing, where r_2 is the radius of the second moment of wing area, defined by $r_2=(\int_S r^2 \mathrm{d}S/S)^{1/2}$, where r is the radial position along the wing and S is the wing area. The wing length R is $2.76c$, and r_2 is $1.6c$ or $0.58R$, where c is the mean chord length.

The flapping motion considered here is an idealized one, which is similar to that considered by Dickinson et al. (1999) and Sun and Tang (2002) in their studies on unsteady lift mechanisms. An up- or downstroke consists of the following three parts, as shown in Fig. 1B: pitching-down rotation and translational acceleration at the beginning of the stroke, translation at constant speed and constant angle of attack during the middle of the stroke, and pitching-up rotation and translational deceleration at the end of the stroke. The translational velocity is denoted by u_t, which takes a constant value of U_m except at the beginning and near the end of a stroke. During the acceleration at the beginning of a stroke, u_t is given by:

$$u_t^+ = U_m^+ \sin[\pi(\tau - \tau_0)/\Delta\tau_t]; \quad \tau_0 \leqslant \tau \leqslant [\tau_0 + (\Delta\tau_t/2)] , \quad (1)$$

where $u_t^+=U_t/U$ (U is the mean value of u_t over a stroke and is used as reference velocity and u_t^+ is the non-dimensional translational velocity of the wing), $U_m^+=U_m/U$ (U_m^+ is the maximum of u_t^+), $\tau=tU/c$ (t is dimensional time and τ is the non-dimensional time), τ_0 is the non-dimensional time at which the stroke starts and $\tau_0+(\Delta\tau_t/2)$ is the time at which the acceleration at the beginning of the stroke finishes. $\Delta\tau_t$ is the duration of deceleration/acceleration around stroke reversal. Near the end of the stroke, the wing decelerates from $u_t^+=U_m^+$ to $u_t^+=0$ according to:

$$u_t^+ = U_m^+ \sin\left\{\frac{\pi}{\Delta\tau_t}[\tau - \tau_1 + (\Delta\tau_t/2)]\right\}; \quad \tau_1 \leqslant \tau \leqslant [\tau_1 + (\Delta\tau_t/2)] , \quad (2)$$

where τ_1 is the non-dimensional time at which the deceleration starts. The azimuth-rotational speed of the wing is related to u_t. Denoting the azimuthal-rotational speed as $\dot{\phi}$, we have $\dot{\phi}(\tau)=u_t/r_2$.

The angle of attack of the wing is denoted by α. It also takes a constant value except at the beginning or near the end of a stroke. The constant value is denoted by α_m. Around the stroke reversal, α changes with time and the angular velocity $\dot{\alpha}$ is given by:

$$\dot{\alpha}^+ = 0.5\dot{\alpha}_0^+\{1 - \cos[2\pi(\tau - \tau_r)/\Delta\tau_r]\}; \quad \tau_r \leqslant \tau \leqslant (\tau_r + \Delta\tau_r) , \quad (3)$$

where the non-dimensional form $\dot{\alpha}^+=\dot{\alpha}c/U$, $\dot{\alpha}_0^+$ is a constant, τ_r is the time at which the rotation starts and $\Delta\tau_r$ is the time interval over which the rotation lasts. In the time interval $\Delta\tau_r$, the wing rotates from $\alpha=\alpha_m$ to $\alpha=180°-\alpha_m$. Therefore, when α_m and $\Delta\tau_r$ are specified, $\dot{\alpha}_0^+$ can be determined (around the next stroke reversal, the wing would rotate from $\alpha=180°-\alpha_m$ to $\alpha=\alpha_m$; the sign of the right-hand side of equation 3 should then be reversed). The axis of the pitching rotation is located $0.2c$ from the leading edge of the wing. $\Delta\tau_r$ is termed wing rotation duration (or flip duration), and τ_r is termed the rotation (or flip) timing, When τ_r is chosen such that the majority of the wing rotation is conducted near the end of a stroke, it is called advanced rotation; when τ_r is chosen such that half the wing rotation is conducted near the end of a stroke and half at the beginning of the next stroke, it is called symmetrical rotation; when τ_r is chosen such that the major part of the wing rotation is delayed to the beginning of the next stroke, it is called delayed rotation.

In the flapping motion described above, the mean flapping velocity U, velocity at midstroke U_m, angle of attack at midstroke α_m, deceleration/acceleration duration $\Delta\tau_t$, wing rotation duration $\Delta\tau_r$, period of the flapping cycle τ_c and flip timing τ_r must be given. These parameters will be determined using available flight data, together with the force balance condition of the flight.

The Navier–Stokes equations and the computational method

The flow equations and computational method used in the present study are the same as in a recent paper (Sun and Tang, 2002). Therefore, only an outline of the method is given here. The governing equations of the flow are the three-dimensional incompressible unsteady Navier–Stokes equations. Written in the inertial coordinate system $OXYZ$ and non-dimensionalized, they are as follows:

$$\frac{\partial u}{\partial X} + \frac{\partial v}{\partial Y} + \frac{\partial w}{\partial Z} = 0 , \quad (4)$$

$$\frac{\partial u}{\partial \tau} + u\frac{\partial u}{\partial X} + v\frac{\partial u}{\partial Y} + w\frac{\partial u}{\partial Z} = -\frac{\partial p}{\partial X} + \frac{1}{Re}\left(\frac{\partial^2 u}{\partial X^2} + \frac{\partial^2 u}{\partial Y^2} + \frac{\partial^2 u}{\partial Z^2}\right) , \quad (5)$$

$$\frac{\partial v}{\partial \tau} + u\frac{\partial v}{\partial X} + v\frac{\partial v}{\partial Y} + w\frac{\partial v}{\partial Z} = -\frac{\partial p}{\partial Y} + \frac{1}{Re}\left(\frac{\partial^2 v}{\partial X^2} + \frac{\partial^2 v}{\partial Y^2} + \frac{\partial^2 v}{\partial Z^2}\right) , \quad (6)$$

$$\frac{\partial w}{\partial \tau} + u\frac{\partial w}{\partial X} + v\frac{\partial w}{\partial Y} + w\frac{\partial w}{\partial Z} = -\frac{\partial p}{\partial Z} + \frac{1}{Re}\left(\frac{\partial^2 w}{\partial X^2} + \frac{\partial^2 w}{\partial Y^2} + \frac{\partial^2 w}{\partial Z^2}\right) , \quad (7)$$

where u, v and w are three components of the non-dimensional fluid velocity and p is the non-dimensional fluid pressure. In the non-dimensionalization, U, c and c/U are taken as reference velocity, length and time, respectively. Re in equations 5–7 denotes the Reynolds number and is defined as $Re=cU/\nu$, where ν is the kinematic viscosity of the fluid.

In the flapping motion considered in the present paper, the wing conducts translational motion (azimuthal rotation) and pitching rotation. To calculate the flow around a body performing unsteady motion (such as the present flapping wing), one approach is to write and solve the governing

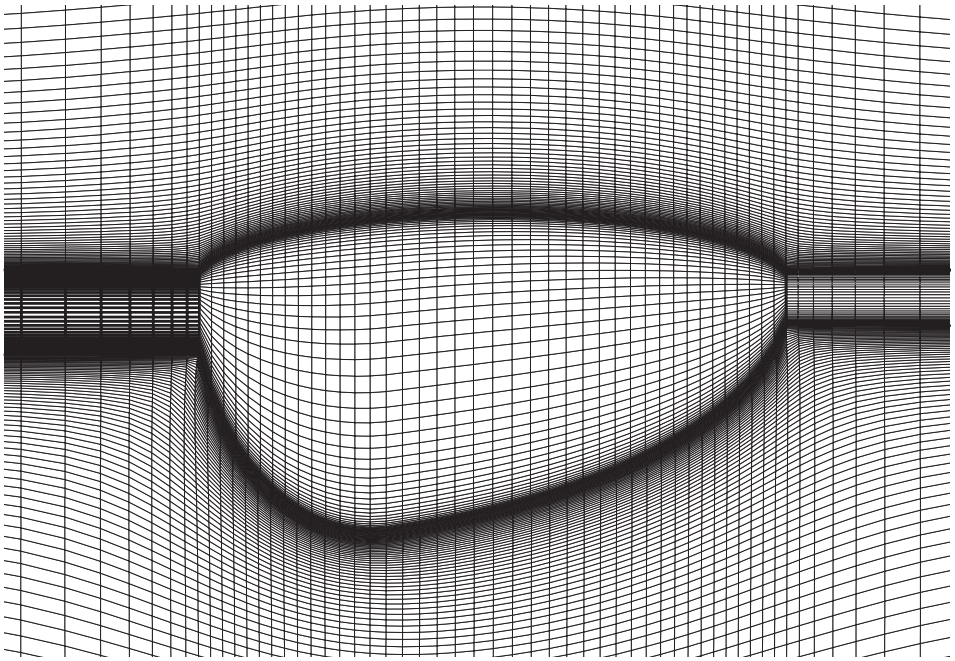

Fig. 2. The wing planform and a portion of the body-conforming grid near the wing in the z=0 plane (see Fig. 1A for a definition of this plane).

equations in a body-fixed, non-inertial reference frame with inertial force terms added to the equations. Another approach is to write and solve the governing equations in an inertial reference frame. By using a time-dependent coordinate transformation and the relationship between the inertial and non-inertial reference frames, a body-conforming computational grid in the inertial reference frame (which varies with time) can be obtained from a body-conforming grid in the body-fixed, non-inertial frame, which needs to be generated only once. This approach has some advantages. It does not need special treatment on the far-field boundary conditions and, moreover, since no extra terms are introduced into the equations, existing numerical methods can be applied directly to the solutions of the equations. This approach is employed here.

The flow equations are solved using the algorithm developed by Rogers and Kwak (1990) and Rogers et al. (1991). The algorithm is based on the method of artificial compressibility, which introduces a pseudotime derivative of pressure into the continuity equation. Time accuracy in the numerical solutions is achieved by subiterating in pseudotime for each physical time step. The algorithm uses a third-order flux-difference splitting technique for the convective terms and a second-order central difference for the viscous terms. The time derivatives in the momentum equation are differenced using a second-order, three-point, backward-difference formula. The algorithm is implicit and has second-order spatial and time accuracy. For details of the algorithm, see Rogers and Kwak (1990) and Rogers et al. (1991). A body-conforming grid was generated using a Poisson solver based on the work of Hilgenstock (1988). The grid topology used in this work was an O–H grid topology. A portion of the grid used for the wing is shown in Fig. 2.

Description of the coordinate systems

In both the flow calculation method outlined above and the force and moment calculations below, two coordinate systems are needed. They are described as follows. One is the inertial coordinate system *OXYZ*. The origin *O* is at the root of the wing. The *X* and *Y* axes are in the horizontal plane with the *X* axis positive aft, the *Y* axis positive starboard and the *Z* axis positive vertically up (see Fig. 1A). The second is the body-fixed coordinate system *oxyz*. It has the same origin as the inertial coordinate system, but it rotates with the wing. The *x* axis is parallel to the wing chord and positive aft, and the *y* axis is on the pitching-rotation axis of the wing and positive starboard (see Fig. 1A). In terms of the Euler angles α and ϕ (defined in Fig. 1A), the relationship between these two coordinate systems is given by:

$$\begin{pmatrix} x \\ y \\ z \end{pmatrix} = \begin{bmatrix} \cos\alpha\cos\phi & \sin\phi\cos\alpha & -\sin\alpha \\ -\sin\phi & \cos\phi & 0 \\ \sin\alpha\cos\phi & \sin\alpha\sin\phi & \cos\alpha \end{bmatrix} \begin{pmatrix} X \\ Y \\ Z \end{pmatrix}, \qquad (8)$$

and

$$\begin{pmatrix} X \\ Y \\ Z \end{pmatrix} = \begin{bmatrix} \cos\alpha\cos\phi & -\sin\phi & \cos\phi\sin\alpha \\ \sin\phi\cos\alpha & \cos\alpha & \sin\phi\sin\alpha \\ -\sin\alpha & 0 & \cos\alpha \end{bmatrix} \begin{pmatrix} x \\ y \\ z \end{pmatrix}. \qquad (9)$$

Evaluation of the aerodynamic forces

Once the Navier–Stokes equations have been numerically solved, the fluid velocity components and pressure at discretized grid points for each time step are available. The aerodynamic force acting on the wing is contributed by the pressure and the viscous stress on the wing surface. Integrating

the pressure and viscous stress over the wing surface at a time step gives the total aerodynamic force acting on the wing at the corresponding instant in time. The lift of the wing, L, is the component of the total aerodynamic force perpendicular to the translational velocity and is positive when directed upwards. The drag, D, is the component of the total aerodynamic force parallel to the translational velocity and is positive when directed opposite to the direction of the translational velocity of the downstroke. The lift and drag coefficients, denoted by C_L and C_D, respectively, are defined as follows:

$$C_L = \frac{L}{0.5\rho U^2 S} , \tag{10}$$

$$C_D = \frac{D}{0.5\rho U^2 S} , \tag{11}$$

where ρ is the fluid density.

Evaluation of the aerodynamic torque and power

The moment around the root of a wing (point o) due to the aerodynamic forces, denoted by $-\mathbf{M_a}$, can be written as follows (assuming that the thickness of the wing is very small):

$$\begin{aligned} -\mathbf{M_a} &= \int_S \mathbf{r} \times \mathbf{F} \mathrm{d}S \\ &\approx -\int_S (yf_z\mathbf{i} - xf_z\mathbf{j} - yf_x\mathbf{k})\mathrm{d}S , \end{aligned} \tag{12}$$

where S is the wing surface area, $\mathbf{F}$ is the aerodynamic force in unit wing area, $\mathbf{r}$ is the distance vector, f_x, f_y and f_z are the three components of $\mathbf{F}$ in the $oxyz$ coordinate system, x, y and z are the three components of $\mathbf{r}$, and $\mathbf{i}$, $\mathbf{j}$ and $\mathbf{k}$ are the unit vectors of the coordinate system $oxyz$ (see Fig. 3). In equation 12, f_y, the component of $\mathbf{F}$ along the wing span, is neglected and f_x and f_z can be obtained from the solution of the flow equations. The angular velocity vector of the wing, $\mathbf{\Omega}$, has the following three components in the $oxyz$ coordinate system:

$$\mathbf{\Omega} = (-\dot{\phi}\sin\alpha,\ \dot{\alpha},\ \dot{\phi}\cos\alpha) . \tag{13}$$

The power required to overcome the aerodynamic moments, called aerodynamic power P_a, can be written as:

$$\begin{aligned} P_a &= \mathbf{M_a} \cdot \mathbf{\Omega} \\ &= \int_S (yf_z\dot{\phi}\sin\alpha + xf_z\dot{\alpha} + yf_x\dot{\phi}\cos\alpha)\mathrm{d}S \\ &= Q_{a,t}\dot{\phi} + Q_{a,r}\dot{\alpha} , \end{aligned} \tag{14}$$

where

$$Q_{a,t} = \int_S y(f_z\sin\alpha + yf_x\cos\alpha)\mathrm{d}S , \tag{15}$$

$$Q_{a,r} = \int_S xf_z\mathrm{d}S . \tag{16}$$

$Q_{a,t}$ is the torque around the axis of azimuthal rotation and is due to the aerodynamic drag. It is termed the aerodynamic torque for translation. Q_{ar} is the torque around the axis of pitching rotation and is due to the aerodynamic pitching moment. It is termed the aerodynamic torque for rotation. The coefficients of the aerodynamic torques are defined as follows:

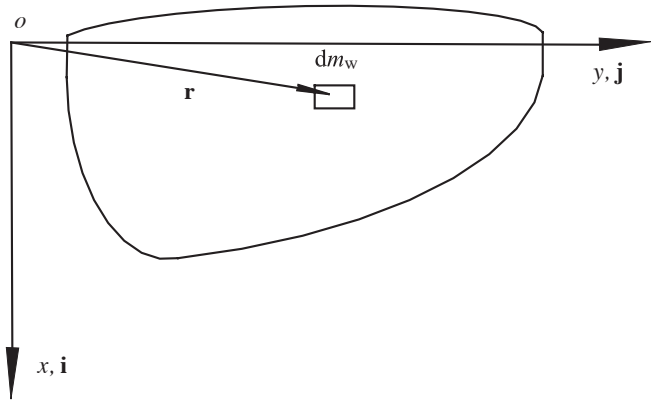

Fig. 3. Diagram showing how the moments and product of inertia are computed. o, x, y, coordinates in wing-fixed frame of reference; $\mathrm{d}m_w$, mass element of the wing; $\mathbf{r}$, vector distance between point o and a mass element of the wing; $\mathbf{i}$, $\mathbf{j}$, unit vectors in the x and y directions, respectively.

$$C_{Q,a,t} = \frac{Q_{a,t}}{0.5\rho U^2 Sc} ; \tag{17}$$

$$C_{Q,a,r} = \frac{Q_{a,r}}{0.5\rho U^2 Sc} . \tag{18}$$

The aerodynamic power coefficient is defined as:

$$C_{P,a} = \frac{P_a}{0.5\rho U^3 S} \tag{19}$$

and can be written as:

$$C_{P,a} = C_{Q,a,t}\dot{\phi}^+ + C_{Q,a,r}\dot{\alpha}^+ , \tag{20}$$

where $\dot{\phi}^+$ is the non-dimensional-angular velocity of azimuthal rotation.

Evaluations of the inertial torques and power

The moments and products of inertia of the mass of a wing, with respect to the $oxyz$ coordinate system (see Fig. 3), can be written as follows, assuming that the thickness of the wing is very small:

$$I_{xx} = \int(y^2 + z^2)\mathrm{d}m_w \approx \int y^2\mathrm{d}m_w , \tag{21}$$

$$I_{yy} = \int(z^2 + x^2)\mathrm{d}m_w \approx \int x^2\mathrm{d}m_w , \tag{22}$$

$$I_{zz} = \int(x^2 + y^2)\mathrm{d}m_w , \tag{23}$$

$$I_{xy} = \int xy\mathrm{d}m_w , \tag{24}$$

$$I_{xz} = \int xz\mathrm{d}m_w \approx 0 , \tag{25}$$

$$I_{yz} = \int yz\mathrm{d}m_w \approx 0 , \tag{26}$$

where $\mathrm{d}m_w$ is a mass element of the wing. The angular

momentum of the wing **H** and its three components in the *oxyz* coordinate system are as follows:

$$\mathbf{H} = -\mathbf{i}(I_{xx}\dot{\phi}\sin\alpha + I_{xy}\dot{\alpha}) + \mathbf{j}(I_{yy}\dot{\alpha} + I_{xy}\dot{\phi}\sin\alpha) + \mathbf{k}I_{zz}\dot{\phi}\cos\alpha\,, \tag{27}$$

where **i**, **j** and **k** are unit vectors in the x, y and z directions, respectively. The inertial moment of the wing, $\mathbf{M_i}$, is:

$$\mathbf{M_i} = \left(\frac{d\mathbf{H}}{dt}\right)_{xyz} + \mathbf{\Omega}\times\mathbf{H} = m_i{}^x\mathbf{i} + m_i{}^y\mathbf{j} + m_i{}^z\mathbf{k}\,, \tag{28}$$

where $(d\mathbf{H}/dt)_{xyz}$ denotes the time derivative of the vector as observed in the rotating system and $m_i{}^x$, $m_i{}^y$ and $m_i{}^z$, the x, y and z components of $\mathbf{M_i}$, respectively, are as follows:

$$m_i{}^x = -\mathbf{i}[I_{xx}\ddot{\phi}\sin\alpha + I_{xy}(\dot{\phi}^2\sin\alpha\cos\alpha + \ddot{\alpha})]\,, \tag{29}$$

$$m_i{}^y = \mathbf{j}(I_{yy}\ddot{\alpha} + I_{xy}\ddot{\phi}\sin\alpha + I_{yy}\dot{\phi}^2\sin\alpha\cos\alpha)\,, \tag{30}$$

$$m_i{}^z = \mathbf{k}[I_{zz}\ddot{\phi}\cos\alpha - 2I_{yy}\dot{\phi}\dot{\alpha}\sin\alpha + I_{xy}(\dot{\alpha}^2 - \dot{\phi}^2\sin^2\alpha)]\,, \tag{31}$$

where $\ddot{\phi}$ and $\ddot{\alpha}$ are the angular acceleration of the azimuthal and pitching rotations, respectively. In deriving equation 28, $I_{yy}\approx I_{zz}-I_{zz}$ was used. The inertial power of the wing is written as follows:

$$\begin{aligned} P_i &= \mathbf{M_i}\cdot\mathbf{\Omega} \\ &= -m_i{}^x\dot{\phi}\sin\alpha + m_i{}^y\dot{\alpha} + m_i{}^z\dot{\phi}\cos\alpha\,, \\ &= (-m_i{}^x\sin\alpha + m_i{}^z\cos\alpha)\dot{\phi} + m_i{}^y\dot{\alpha} \\ &= Q_{i,t}\dot{\phi} + Q_{i,r}\dot{\alpha}\,, \end{aligned} \tag{32}$$

where

$$\begin{aligned} Q_{i,t} &= -m_i{}^x\sin\alpha + m_i{}^z\cos\alpha \\ &= (I_{xx}\sin^2\alpha + I_{zz}\cos^2\alpha)\ddot{\phi} + I_{xy}(\dot{\alpha}^2\cos\alpha + \ddot{\alpha}\sin\alpha) \\ &\quad -2I_{yy}\dot{\phi}\dot{\alpha}\sin\alpha\cos\alpha\,; \end{aligned} \tag{33}$$

$$\begin{aligned} Q_{i,r} &= m_i{}^y \\ &= I_{yy}\ddot{\alpha} + I_{xy}\ddot{\phi}\sin\alpha + I_{yy}\dot{\phi}^2\sin\alpha\cos\alpha\,. \end{aligned} \tag{34}$$

$Q_{i,t}$ is the inertial torque around the axis of azimuthal rotation and is termed the inertial torque for translation. $Q_{i,r}$ is the inertial torque around the axis of pitching rotation and is termed the inertial torque for rotation. The coefficients of P_i, $Q_{i,t}$ and $Q_{i,r}$ are denoted by $C_{P,i}$, $C_{Q,i,t}$ and $C_{Q,i,r}$, respectively, and are defined in the same way as the coefficients of the aerodynamic power and aerodynamic torques. From equation 32, the inertial power coefficient can be written as:

$$C_{P,i} = C_{Q,i,t}\dot{\phi}^+ + C_{Q,i,r}\dot{\alpha}^+ \tag{35}$$

and the expressions for $C_{Q,i,t}$ and $C_{Q,i,r}$ are as follows:

$$C_{Q,i,t} = \frac{I_{zz}}{0.5\rho Sc^3}\left\{\left[\left(\cos^2\alpha + \frac{I_{xx}}{I_{zz}}\sin^2\alpha\right)\ddot{\phi}^+\right] + \frac{I_{xy}}{I_{zz}}(\dot{\alpha}^{+2}\cos\alpha + \ddot{\alpha}^+\sin\alpha) - 2\frac{I_{yy}}{I_{zz}}\dot{\phi}^+\dot{\alpha}^+\sin\alpha\cos\alpha\right\}\,; \tag{36}$$

$$C_{Q,i,r} = \frac{I_{yy}}{0.5\rho Sc^3}\left(\ddot{\alpha}^+ + \frac{I_{xy}}{I_{yy}}\ddot{\phi}^+\sin\alpha + \dot{\phi}^{+2}\sin\alpha\cos\alpha\right)\,, \tag{37}$$

where $\ddot{\phi}^+$ and $\ddot{\alpha}^+$ are the non-dimensional angular acceleration of the azimuthal and pitching rotations, respectively. Using the values of I_{xx}, I_{yy}, I_{zz} and I_{xy} given in the next section, $C_{Q,i,t}$ and $C_{Q,i,r}$ can be written as:

$$C_{Q,i,t} = 4.6[(\cos^2\alpha + 0.91\sin^2\alpha)\ddot{\phi}^+ + 0.19(\dot{\alpha}^{+2}\cos\alpha + \ddot{\alpha}^+\sin\alpha) - 0.17\dot{\phi}^+\dot{\alpha}^+\sin\alpha\cos\alpha]\,, \tag{38}$$

$$C_{Q,i,r} = 0.40(\ddot{\alpha}^+ + 2.14\ddot{\phi}^+\sin\alpha + \dot{\phi}^{+2}\sin\alpha\cos\alpha)\,. \tag{39}$$

From equations 36 and 37, or equations 38 and 39, it can be seen that the translational motion also contributes to the rotational inertial torque and *vice versa*. Since I_{xy} is over twice as large as I_{yy}, the contribution from the translational acceleration $\ddot{\phi}^+$ to the rotational inertial torque can be larger than that from the rotational acceleration $\ddot{\alpha}^+$.

Evaluation of the total mechanical power

The total mechanical power of the wing, P, is the power required to overcome the combination of the aerodynamic and inertial torques and can be written as:

$$P = (\mathbf{M_a} + \mathbf{M_i})\cdot\mathbf{\Omega}\,. \tag{40}$$

Henceforth, it is termed simply the power. Combining equations 20 and 35, the non-dimensional power coefficient (represented by C_P), can be written as follows:

$$C_P = C_{P,t} + C_{P,r} \tag{41}$$

where

$$C_{P,t} = (C_{Q,a,t} + C_{Q,i,t})\dot{\phi}^+\,, \tag{42}$$

$$C_{P,r} = (C_{Q,a,r} + C_{Q,i,r})\dot{\alpha}^+\,. \tag{43}$$

$C_{P,t}$ is the coefficient of power for translation and $C_{P,r}$ the coefficient of power for rotation.

Data for hovering flight in Drosophila virilis

Data for free hovering flight of the fruit fly *Drosophila virilis* Sturtevant were taken from Weis-Fogh (1973), which were derived from Vogel's studies of tethered flight (Vogel, 1966). Insect weight was 1.96×10^{-5} N, wing mass was 2.4×10^{-6} g (for one wing), wing length R was 0.3 cm, the area of both wings S_t was 0.058 cm^2, mean chord length c was 0.097 cm, stroke amplitude Φ was 2.62 rad and stroke frequency n was 240 s^{-1}.

From the above data, the mean translational velocity of the wing U (the reference velocity), the Reynolds number Re, the non-dimensional period of the flapping cycle τ_c and mean lift coefficient required for supporting the insect's weight $\bar{C}_{L,w}$ were calculated as follows: $U=2\Phi nr_2=218.7$ cm s^{-1}; $Re=cU/\nu=147$ ($\nu=0.144$ cm^2 s^{-1}); $\tau_c=(1/n)/(U/c)=8.42$; $\bar{C}_{L,w}=1.96\times10^{-5}/0.5\rho U^2S_t=1.15$ ($\rho=1.23\times10^{-3}$ g cm^{-3}). Note that, in our previous work (Sun and Tang, 2002), a smaller $\bar{C}_{L,w}$ (approximately 0.8) was obtained for the same insect under the same flight conditions. This is because a larger reference velocity, the velocity at midstroke, was used there. The moments and product of inertia were calculated by assuming that the wing mass was uniformly distributed over the wing planform, and the results were as follows:

I_{xx}=0.721×10^{-7} g cm^2; I_{yy}=0.069×10^{-7} g cm^2; I_{zz}=0.790×10^{-7} g cm^2; I_{xy}=0.148×10^{-7} g cm^2.

Results and discussion

Test of the flow solver

The code used here, which is based on the flow-computational method outlined above, was developed by Lan and Sun (2001a). It was verified by the analytical solutions of the boundary layer flow on a flat plate (Lan and Sun, 2001a) and the flow at the beginning of a suddenly started aerofoil (Lan and Sun, 2001b) and tested by comparing the calculated and measured steady-state pressure distributions on a wing (Lan and Sun, 2001a). To establish further the validity of the code in calculating the unsteady aerodynamic force on flapping wings, we present below a comparison between our calculated results and the experimental data of Dickinson et al. (1999). In our previous work on the fruit fly wing in flapping motion (Sun and Tang, 2002), calculated results using this code were compared with the experimental data, but the wing aspect ratio was not the same as that used in the experiments and only one case was compared.

Measured unsteady lift in Dickinson et al. (1999) was presented in dimensional form. For comparison, we need to convert it into the lift coefficient. In their experiment, the fluid density ρ was 0.88×10^3 kg m^{-3}, the model wing length R was 0.25 m and the wing area S was 0.0167 m^2. The speed at the wing tip during the constant-speed translational phase of a stroke, given in Fig. 3D of Dickinson et al. (1999), was 0.235 m s^{-1} and, therefore, the reference speed (mean speed at r_2=0.58R) was calculated to be U=0.118 m s^{-1}. From the above data, 0.5ρU^2S=0.102 N. Using the definition of C_L (equation 10), the lift in Fig. 3A of Dickinson et al. (1999) can be converted to C_L (Fig. 4) and compared with the calculated C_L for the cases of advanced rotation (Fig. 4A), symmetrical rotation (Fig. 4B) and delayed rotation (Fig. 4C). The aspect ratio of the wing in the experiment was calculated as R^2/S=3.74, and a wing of the same aspect ratio was used in the calculation. The magnitude and trends with variation over time of the calculated C_L are in reasonably good agreement with the measured values.

In the above calculation, the computational grid had dimensions of 93×109×71 in the normal direction, around the wing section and in the spanwise direction, respectively. The normal grid spacing at the wall was 0.002. The outer boundary was set at 10 chord lengths from the wing. The time step was 0.02. Detailed study of the numerical variables such as grid size, domain size, time step, etc., was conducted in our previous work on the unsteady lift mechanism of a flapping fruit fly wing (Sun and Tang, 2002), where it was shown that the above values for the numerical variables were appropriate for the flow calculation. Therefore, in the following calculation, the same set of numerical variables was used.

Force balance in hovering flight

Since we wanted to study the power requirements for balanced flight, we first investigated the force balance. For the flapping motion considered in the present study, the mean drag on the wing over each flapping cycle was zero, and the horizontal force was balanced. Therefore, we needed only to consider under what conditions the weight of the insect was balanced by the mean lift.

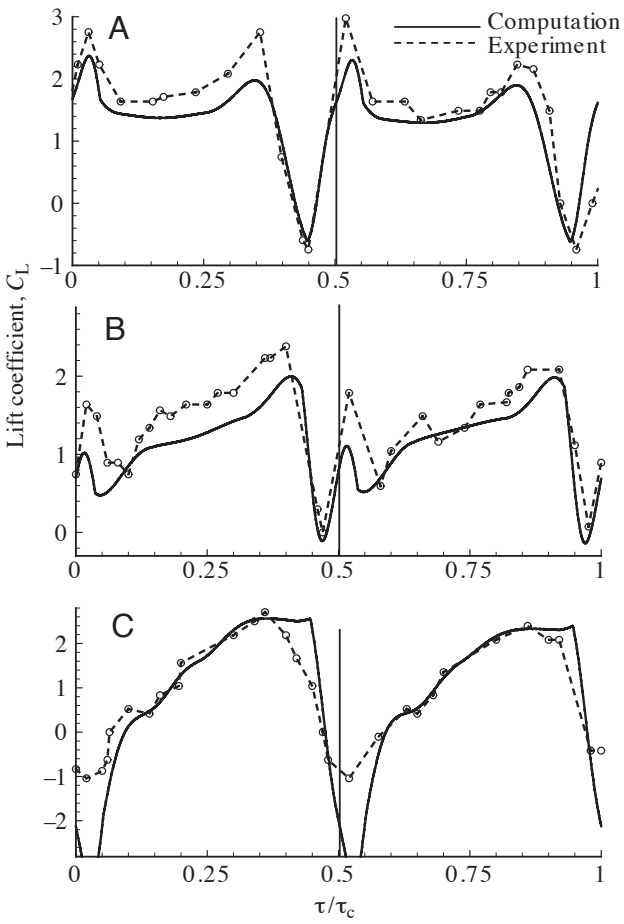

Fig. 4. Comparison of the calculated lift coefficient C_L with the measured C_L. The experimental data are reproduced from Fig. 3 of Dickinson et al. (1999). (A) Advanced rotation. (B) Symmetrical rotation. (C) Delayed rotation. τ, non-dimensional time; τ_c, non-dimensional period of one flapping cycle.

As noted above, the kinematic parameters required to describe the wing motion are U, U_m^+, τ_c, $\Delta\tau_t$, $\Delta\tau_r$, τ_r and α_m. Of these, U and τ_c were determined above using the flight data given by Weis-Fogh (1973). Ennos (1989) made observations of the free forward flight of *Drosophila melanogaster* (the flight was approximately balanced). His data (his Figs 6D, 7A) showed that symmetrical rotation was employed by the insect. Data on the hovering flight of craneflies, hoverflies and droneflies also showed that symmetrical rotation was employed by these insects (see Figs 8, 9 and 12, respectively, of Ellington, 1984a). Therefore, it was assumed here that symmetrical rotation was employed in hovering flight in *Drosophila virilis*; as a result, τ_r was determined. From the data of Ennos (1989) and Ellington (1984a), the deceleration/

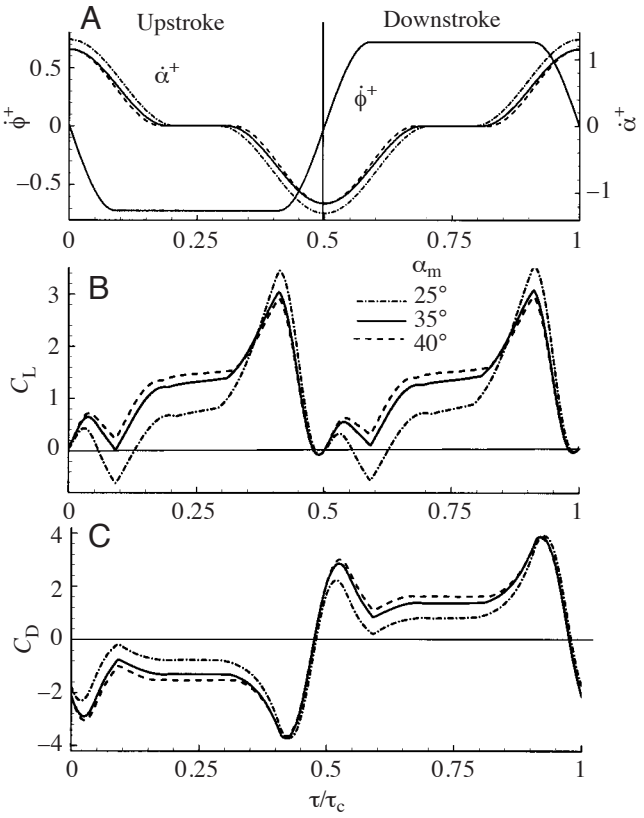

Fig. 5. Non-dimensional angular velocity of pitching rotation $\dot{\alpha}^+$ and azimuthal rotation $\dot{\phi}^+$ (A), lift coefficient C_L (B) and drag coefficient C_D (C) *versus* time during one cycle for three midstroke angles of attack α_m (symmetrical rotation, non-dimensional duration of wing rotation $\Delta\tau_r=0.36\tau_c$). τ_c, non-dimensional period of one flapping cycle; τ, non-dimensional time.

acceleration duration $\Delta\tau_t$ was estimated to be approximately $0.2\tau_c$. We assumed that $\Delta\tau_t=0.18\tau_c$ (this value was used in previous studies on unsteady force mechanism of the fruit fly wing; Dickinson et al., 1999; Sun and Tang, 2002). Using $\Delta\tau_t$ and U, U_m^+ could be determined.

Dickinson et al. (1999) and Sun and Tang (2002) used $\Delta\tau_r\approx0.36\tau_c$. In the present study, we first assumed $\Delta\tau_r\approx0.36\tau_c$ and then investigated the effects of varying $\Delta\tau_r$. At this point, all the kinematic parameters had been determined except α_m, which was determined using the force balance condition.

The calculated lift coefficients *versus* time for three values of α_m are shown in Fig. 5. The mean lift coefficient $\overline{C_L}$ plotted against α_m is shown in Fig. 6. In the range of α_m considered (α_m=25–50°), $\overline{C_L}$ increases with α_m; at α_m=35°, $\overline{C_L}$=1.15, which is the value needed to balance the weight of the insect. At α_m=35°, the mean drag coefficient during an up- or downstroke (represented by $\overline{C_D}$) was calculated to be 1.55, which is significantly larger than $\overline{C_L}$ (=1.15). The lift-to-drag ratio is 1.15/1.55=0.74.

Power requirements

As shown above, at α_m=35°, the insect produced enough lift to support its weight. In the following, we calculated the power

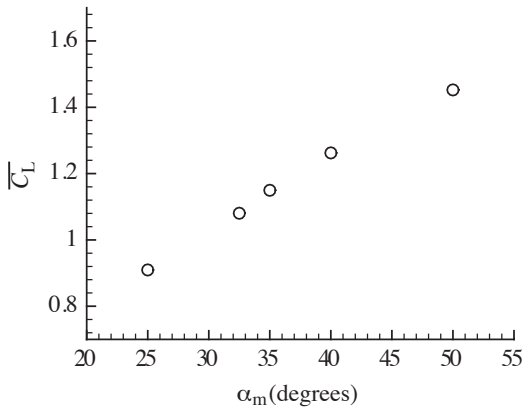

Fig. 6. Mean lift coefficient $\overline{C_L}$ *versus* midstroke angle of attack α_m (symmetrical rotation, non-dimensional duration of wing rotation $\Delta\tau_r=0.36\tau_c$, where τ_c is the non-dimensional period of one flapping cycle).

required to produce this lift and investigated the mechanical power output of insect flight muscle and its mechanochemical efficiency.

Aerodynamic torque

As expressed in equation 20, the aerodynamic power consists of two components, one due to the aerodynamic torque for translation and the other due to the aerodynamic torque for rotation. The coefficients of these two torques, $C_{Q,a,t}$ and $C_{Q,a,r}$, are shown in Fig. 7B. $C_{Q,a,t}$ is much larger than $C_{Q,a,r}$. The $C_{Q,a,t}$ curve is similar in shape to the C_D curve shown in Fig. 5C for obvious reasons.

One might expect that, during the deceleration of the wing near the end of a stroke, $C_{Q,a,t}$ would change sign because of the wing being 'pushed' by the flow behind it. But as seen from Fig. 7B (e.g. during the downstroke), $C_{Q,a,t}$ becomes negative only when the deceleration is almost finished because, while decelerating, the wing rotates around an axis that is near its leading edge. Therefore, a large part of the wing is effectively not in deceleration and does not 'brake' the pushing flow.

Inertial torque

The coefficients of the inertial torques for translation ($C_{Q,i,t}$) and for rotation ($C_{Q,i,r}$) are shown in Fig. 7C. The inertial torques are approximately zero in the middle of a stroke, when the translational and rotational accelerations are zero. At the beginning and near the end of the stroke, the inertial torque for translation has almost the same magnitude as its aerodynamic counterpart. Similar to the case of the aerodynamic torques, the inertial torque for translation is much larger than the inertial torque for rotation.

At the beginning of a stroke, the sign of $C_{Q,i,r}$ is opposite to that of $\dot{\alpha}^+$ (Fig. 7C). Near the end of the stroke, the sign of $C_{Q,i,r}$ is also opposite to that of $\dot{\alpha}^+$. In this part of the stroke, although $\ddot{\alpha}^+$ has the same sign as $\dot{\alpha}^+$, $\ddot{\phi}^+$ has the opposite sign to $\dot{\alpha}^+$. In equation 37, $\ddot{\phi}^+$ is multiplied by I_{xy}, which is much

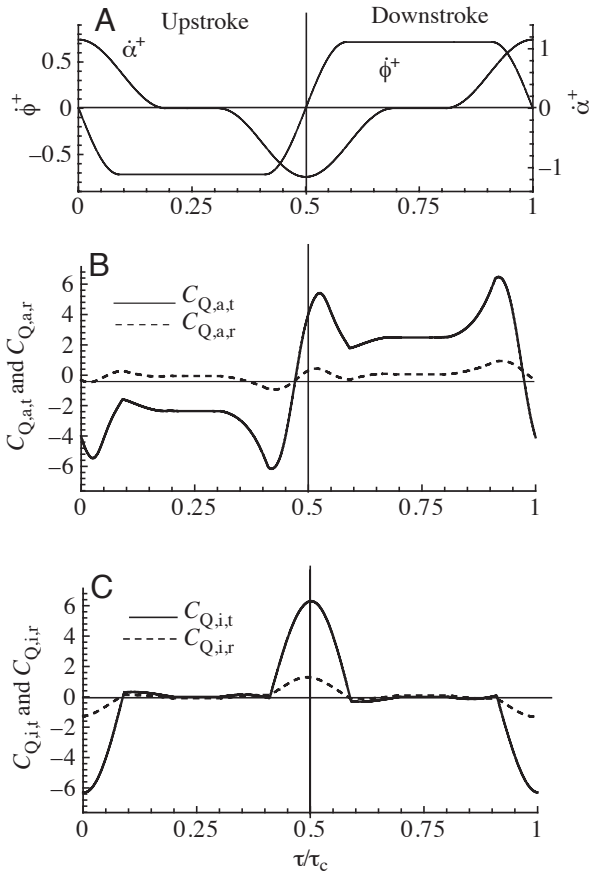

Fig. 7. Non-dimensional angular velocity of pitching rotation $\dot{\alpha}^+$ and azimuthal rotation $\dot{\phi}^+$ (A), aerodynamic (B) and inertial (C) torque coefficients for translation ($C_{Q,a,t}$ and $C_{Q,i,t}$, respectively) and rotation ($C_{Q,a,r}$ and $C_{Q,i,r}$, respectively) *versus* time during one cycle (midstroke angle of attack α_m=35°, symmetrical rotation, non-dimensional duration of wing rotation $\Delta\tau_r$=0.36τ_c). τ_c, non-dimensional period of one flapping cycle; τ, non-dimensional time.

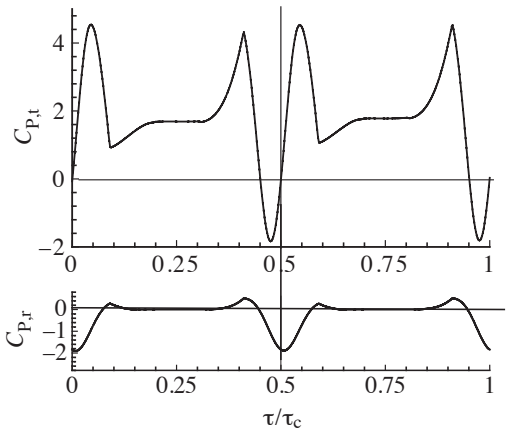

Fig. 8. The power coefficients for translation ($C_{P,t}$) and rotation ($C_{P,r}$) *versus* time during one cycle (midstroke angle of attack α_m=35°, symmetrical rotation, non-dimensional duration of wing rotation $\Delta\tau_r$=0.36τ_c). τ_c, non-dimensional period of one flapping cycle; τ, non-dimensional time.

larger than I_{yy}; thus, its effect dominates over that of other terms in the equation, leading to the above result. This shows that, for the flapping motion considered, the inertial torque of rotation will always contribute to 'negative' work.

Power and work

From the above results for the aerodynamic and inertial torque coefficients, the power coefficients can be computed using equations 41–43. The coefficients of power for translation ($C_{P,t}$) and rotation ($C_{P,r}$) are plotted against time in Fig. 8. $C_{P,t}$ is positive for the majority of a stroke and becomes negative only for a very short period close to the end of the stroke. $C_{P,r}$ is negative at the beginning and near the end of a stroke and is approximately zero in the middle of the stroke. Throughout a stroke, the magnitude of $C_{P,t}$ is much larger than that of $C_{P,r}$. Two large positive peaks in $C_{P,t}$ appear during a stroke. One occurs during the rapid acceleration phase of the stroke as a result of the larger aerodynamic and inertial torques occurring there. The other is in the fast pitching-up rotation phase of the stroke and is due to the large aerodynamic torque there.

Integrating $C_{P,t}$ over the part of a cycle where it is positive gives the coefficient of positive work for translation, which is represented by $C_{W,t}^+$. Integrating $C_{P,t}$ over the part of the cycle where it is negative gives the coefficient of 'negative' work for translation; this is represented by $C_{W,t}^-$. Similar integration of $C_{P,r}$ gives the coefficients of the positive and negative work for rotation; they are denoted by $C_{W,r}^+$ and $C_{W,r}^-$, respectively. The results of the integration are: $C_{W,t}^+$=15.96, $C_{W,t}^-$=–1.00, $C_{W,r}^+$=0.56 and $C_{W,r}^-$=–2.30.

Specific power

The body-mass-specific power, denoted by P^*, is defined as the mean mechanical power over a flapping cycle (or a stroke in the case of normal hovering) divided by the mass of the insect. P^* can be written as follows:

$$P^* = 0.5\rho U^3 S_t (C_W/\tau_c)/m$$
$$= 9.81 U C_W/(\tau_c \bar{C}_{L,w}) , \quad (44)$$

where m is the mass of the insect and C_W is the coefficient of work per cycle ($\bar{C}_{L,w}$=1.15, τ_c=8.421 and U=2.19 m s^{-1}, as discussed above).

When calculating C_W, one needs to consider how the ' negative' work fits into the power budget (Ellington, 1984c). There are three possibilities (Ellington, 1984c; Weis-Fogh, 1972, 1973). One is that the negative power is simply dissipated as heat and sound by some form of an end stop; it can then be ignored in the power budget. The second is that, during the period of negative work, the excess energy can be stored by an elastic element, and this energy can then be released when the wing does positive work. The third is that the flight muscles do negative work (i.e. they are stretched while developing tension, instead of contracting as in 'positive' work), but the negative work uses much less metabolic energy than an equivalent amount of positive work. Of these three possibilities, we calculated C_W (or P^*) on the basis of the

assumption that the muscles act as an end stop. C_W is written as:

$$C_W = C_{W,t}^+ + C_{W,r}^+ . \quad (45)$$

It should be pointed out that, for the insect considered in the present study, the negative work is much smaller than the positive work (see Fig. 8 and below); therefore, C_W calculated by considering the other possibilities will not be very different from that calculated from equation 45.

Using $C_{W,t}^+$ and $C_{W,r}^+$ calculated above, C_W was calculated using equation 45 to be 16.52. The specific power P^* was then calculated using equation 44: P^*=36.7 W kg^{-1}.

Effects of the timing of wing rotation on lift and power

In the flight considered above, symmetrical rotation was employed. Dickinson et al. (1999) showed that the timing of the wing rotation had significant effects on the lift and drag of the wing. It is of interest to see how the lift and the power required change when the timing of wing rotation is varied.

Fig. 9 shows the calculated lift and drag coefficients for the cases of advanced rotation and delayed rotation (results for the case of symmetrical rotation are included for comparison). The value of τ_r used can be read from Fig. 9A. The case of advanced rotation has a larger C_L and C_D than the case of symmetrical rotation, and the case of delayed rotation has a much smaller C_L and a slightly larger C_D than the case of symmetrical rotation. An explanation for the above force behaviours was given by Dickinson et al. (1999) and Sun and Tang (2002). The mean lift coefficient $\overline{C_L}$ for the advanced rotation case is 1.47, 28 % larger than that for the symmetrical rotation case (1.15); $\overline{C_L}$ for the delayed rotation case is only 0.39, which is 66 % smaller than that for the symmetrical rotation case.

The aerodynamic and inertial torque coefficients for the advanced rotation and delayed rotation cases are shown in Figs 10 and 11, respectively. Similar to the symmetrical rotation

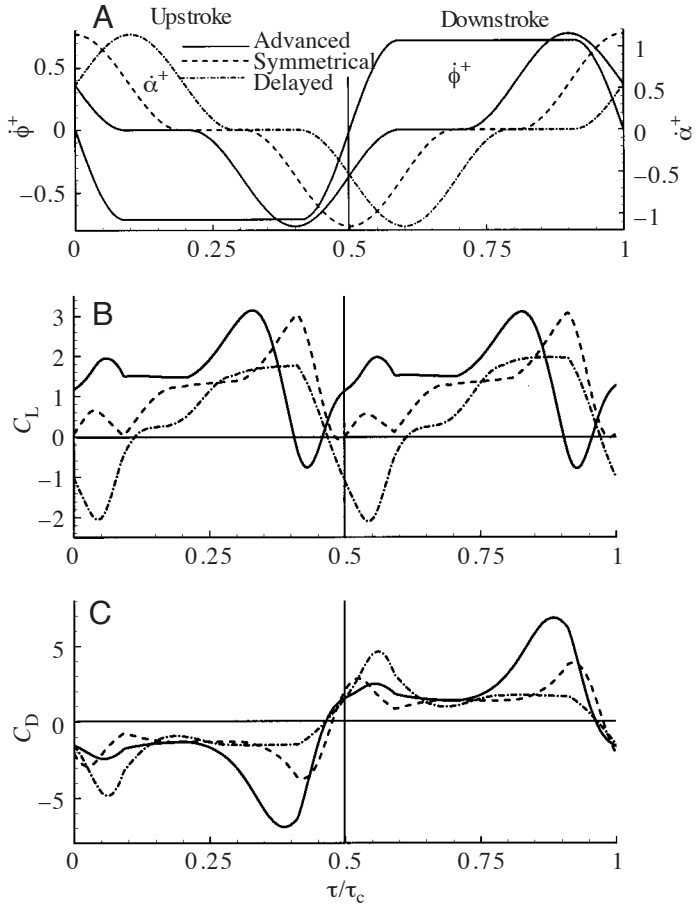

Fig. 9. Non-dimensional angular velocity of pitching rotation $\dot{\alpha}^+$ and azimuthal rotation $\dot{\phi}^+$ (A), lift coefficient C_L (B) and drag coefficient C_D (C) *versus* time during one cycle for three different timings of wing rotation (midstroke angle of attack α_m=35 °, non-dimensional duration of wing rotation $\Delta\tau_r$=0.36τ_c). τ_c, non-dimensional period of one flapping cycle; τ, non-dimensional time.

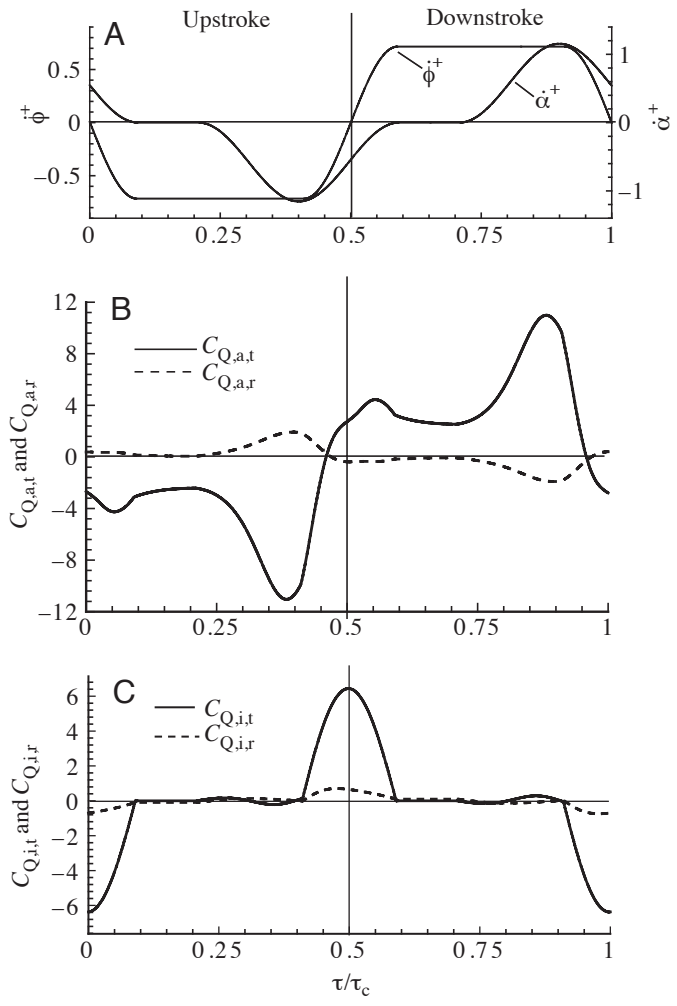

Fig. 10. Non-dimensional angular velocity of pitching rotation $\dot{\alpha}^+$ and azimuthal rotation $\dot{\phi}^+$ (A), aerodynamic (B) and inertial (C) torque coefficients for translation ($C_{Q,a,t}$ and $C_{Q,i,t}$, respectively) and rotation ($C_{Q,a,r}$ and $C_{Q,i,r}$, respectively) *versus* time during one cycle (midstroke angle of attack α_m=35 °, advanced rotation, non-dimensional duration of wing rotation $\Delta\tau_r$=0.36τ_c). τ_c, non-dimensional period of one flapping cycle; τ, non-dimensional time.

case, the $C_{Q,a,t}$ curve for the case of advanced rotation (or delayed rotation) looks like the corresponding C_D curve. For the advanced rotation case, $C_{Q,a,t}$ is much larger than that of the symmetrical rotation case, especially from the middle to the end of the stroke (compare Fig. 10B with Fig. 7B). $C_{Q,i,t}$ is the same as that of the symmetrical rotation case, because the translational acceleration is the same for the two cases (compare Fig. 10C with Fig. 7C). For the delayed rotation case, $C_{Q,a,t}$ is larger than that of the symmetrical rotation case in the early part of a stroke (compare Fig. 11B with Fig. 7B). $C_{Q,i,t}$ is the same as that of the symmetrical rotation case for the same reason as above. Similar to the symmetrical rotation case, for both the advanced and delayed rotation cases, $C_{Q,a,r}$ and $C_{Q,i,r}$ are much smaller than $C_{Q,a,t}$ and $C_{Q,i,t}$, respectively.

The non-dimensional power coefficients for the cases of advanced rotation and delayed rotation are shown in Fig. 12 (the results of symmetrical rotation, taken from Fig. 8, are included for comparison). $C_{P,r}$ is much smaller than $C_{P,t}$ because, as shown in Figs 10 and 11, $C_{Q,a,r}$ and $C_{Q,i,r}$ were much smaller than $C_{Q,a,t}$ and $C_{Q,i,t}$, respectively. $C_{P,t}$ behaves approximately the same as $C_{Q,a,t}$. The most striking feature of Fig. 12 is that $C_{P,t}$ for advanced rotation is much larger than that for symmetrical rotation from the middle to near the end of a stroke.

Integrating the power for the cases of advanced rotation and delayed rotation in the same way as above for the case of symmetrical rotation, the corresponding values of $C_{W,t}^{+}$, $C_{W,t}^{-}$, $C_{W,r}^{+}$ and $C_{W,r}^{-}$ were obtained, from which the work coefficient per cycle, C_W, was calculated. The results are given in Table 1 (results for symmetrical rotation are included for comparison). For the advanced rotation case, C_W is approximately 80 % larger than for symmetrical rotation case. As noted above, $\overline{C_L}$ is 28 % larger than that of the symmetrical rotation case. This shows that advanced rotation can produce more lift but is very energy-demanding. For the delayed rotation case, C_W is approximately 10 % larger than for the symmetrical rotation case but, as noted above, its $\overline{C_L}$ is 66 % smaller; therefore, the energy spent per unit $\overline{C_L}$ is much larger than for the symmetrical rotation case. The above results show that advanced rotation and delayed rotation would be much more costly if used in balanced, long-duration flight.

For reference, we calculated another case in which advanced rotation timing was employed in balanced flight but α_m was

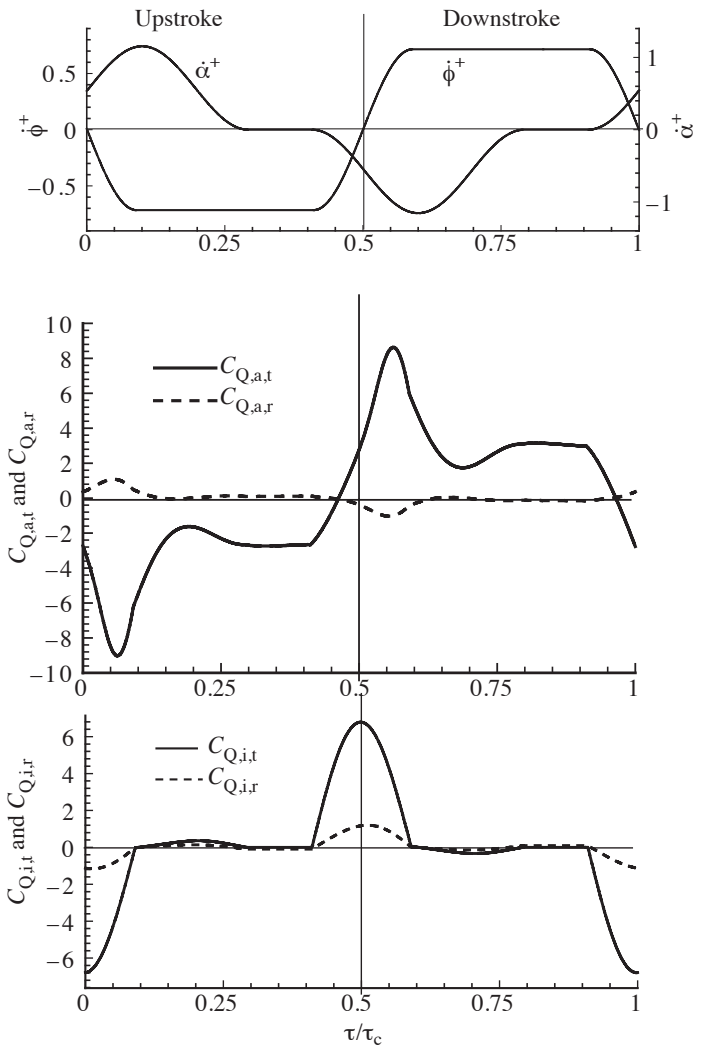

Fig. 11. Non-dimensional angular velocity of pitching rotation $\dot{\alpha}^+$ and azimuthal rotation $\dot{\phi}^+$ (A), aerodynamic (B) and inertial (C) torque coefficients for translation ($C_{Q,a,t}$ and $C_{Q,i,t}$, respectively) and rotation ($C_{Q,a,r}$ and $C_{Q,i,r}$, respectively) *versus* time during one cycle (midstroke angle of attack α_m=35°, delayed rotation, non-dimensional duration of wing rotation $\Delta\tau_r$=0.36τ_c). τ_c, non-dimensional period of one flapping cycle; τ, non-dimensional time.

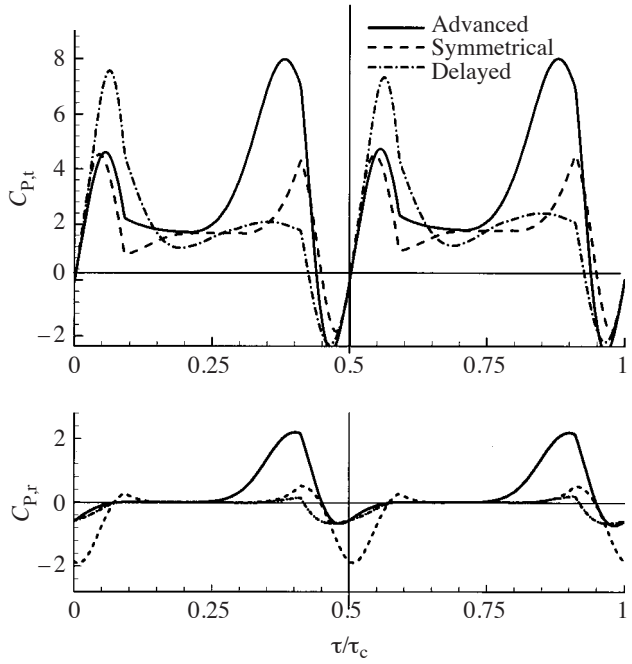

Fig. 12. The power coefficients for translation ($C_{P,t}$) and rotation ($C_{P,r}$) *versus* time during one cycle for the different wing rotation timings (midstroke angle of attack α_m=35°, non-dimensional duration of wing rotation $\Delta\tau_r$=0.36τ_c). τ_c, non-dimensional period of one flapping cycle; τ, non-dimensional time.

Table 1. *Effects of the timing of wing rotation on lift and power ($\Delta\tau_r$=0.36τ_c)*

α_m (degrees)	Rotation timing	$\overline{C_L}$	$C_{W,t}^+$	$C_{W,t}^-$	$C_{W,r}^+$	$C_{W,r}^-$	C_W
35	Symmetrical	1.15	15.96	–1.0	0.56	–2.30	16.52
35	Advanced	1.47	26.08	–1.62	3.48	–0.72	29.56
35	Delayed	0.39	17.70	–1.90	0.14	–2.70	17.84
22	Advanced	1.15	24.74	–1.84	5.36	–0.40	30.10

$\overline{C_L}$, mean lift coefficient; C_W, coefficient of work per cycle; $C_{W,t}^+$ and $C_{W,t}^-$, coefficients of positive and negative work for translation, respectively; $C_{W,r}^+$ and $C_{W,r}^-$, coefficients of positive and negative work for rotation, respectively; α_m, midstroke angle of attack; $\Delta\tau_r$, non-dimensional duration of wing rotation; τ_c, non-dimensional period of one flapping cycle.

decreased to 22 ° so that the mean lift was equal to the weight (Table 1). In this case, C_W was 30.10, which is approximately 82 % larger than for the case employing symmetrical rotation, showing clearly that advanced rotation is very energy-demanding.

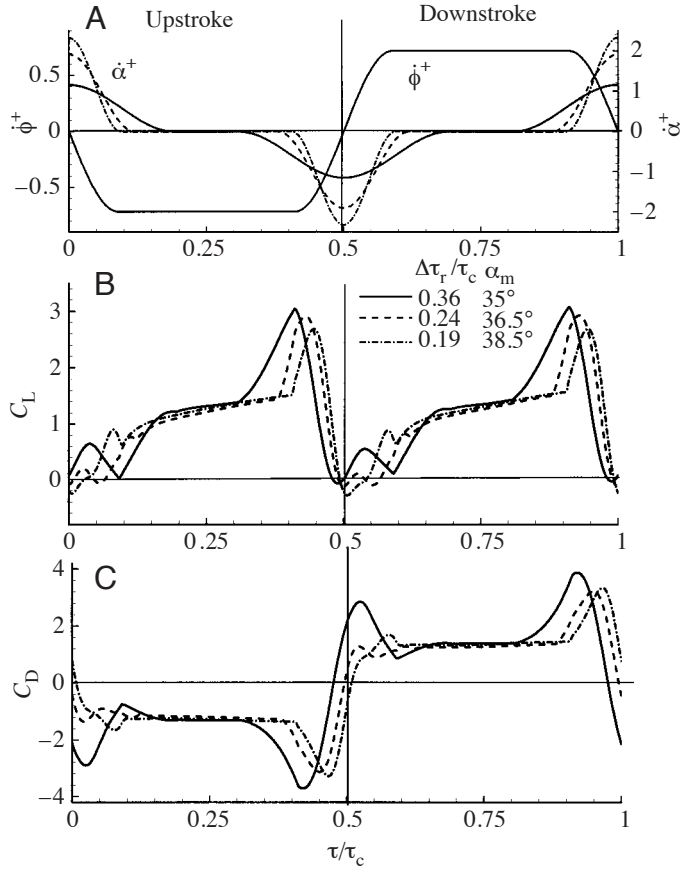

Fig. 13. Non-dimensional angular velocity of pitching rotation $\dot{\alpha}^+$ and azimuthal rotation $\dot{\phi}^+$ (A), lift coefficient C_L (B) and drag coefficient C_D (C) *versus* time during one cycle for three different values of the non-dimensional duration of wing rotation $\Delta\tau_r$. Symmetrical rotation; mean lift coefficient $\overline{C_L}$=1.15 (midstroke angle of attack α_m was adjusted to make the mean lift equal to insect weight). τ_c, non-dimensional period of one flapping cycle; τ, non-dimensional time.

Effects of flip duration

In the above analyses, the duration of wing rotation (or flip duration) was taken as $\Delta\tau_r$=0.36τ_c. Below, the effects of changing the flip duration were investigated. Fig. 13 shows the lift and drag coefficients of the wing for two shorter flip durations $\Delta\tau_r$=0.24τ_c and $\Delta\tau_r$=0.19τ_c, with the above results for $\Delta\tau_r$=0.36τ_c included for comparison. If the flip duration is varied while other parameters are kept unchanged, the mean lift coefficient will change. To maintain the balance between mean lift and insect weight, α_m was therefore adjusted. For $\Delta\tau_r$=0.24τ_c, α_m was changed to 36.5 ° to give a $\overline{C_L}$ of 1.15; for $\Delta\tau_r$=0.19τ_c, α_m was changed to 38.5 °.

From Fig. 13C, it can be seen that, when $\Delta\tau_r$ is decreased, the C_D peak at the beginning of a stroke becomes much smaller and the C_D peak near the end of the stroke is delayed and becomes slightly smaller. A smaller C_D at the beginning of the stroke means reduced aerodynamic power there. Since the wing decelerates near the end of the stroke, delaying the C_D peak at this point means that the peak would occur when the wing has a lower velocity, resulting in reduced aerodynamic power. The power coefficients are shown in Fig. 14; at the beginning and at the end of a stroke, $C_{P,t}$ is smaller for smaller $\Delta\tau_r$.

By integrating the power coefficients in Fig. 14, $C_{W,t}^+$, $C_{W,t}^-$, $C_{W,r}^+$ and $C_{W,r}^-$ were obtained (Table 2). C_W was computed using equation 45, and the results are also shown in Table 2. When $\Delta\tau_r$ is decreased to 0.24τ_c, C_W is 12.96, much smaller than for $\Delta\tau_r$=0.36τ_c. When $\Delta\tau_r$ is further decreased to 0.19τ_c, C_W was slightly greater (13.06). This is because when $\Delta\tau_r$ is decreased to 0.19τ_c, $C_{W,t}^+$ also decreases; however, $C_{W,r}^+$ increases (possibly due to the wing rotation becoming very fast).

For $\Delta\tau_r$=0.24τ_c (which has approximately the same C_W as $\Delta\tau_r$=0.19τ_c), the mass-specific power P^* was computed to be 28.7 W kg^{-1}. If the ratio of the flight muscle mass to the body mass is known, the power per unit flight muscle or muscle-mass-specific power (P_m^*) can be calculated from the body-mass-specific power. Lehmann and Dickinson (1997) obtained a value of 0.3 for the ratio for fruit fly *Drosophila melanogaster*. This value gives:

$$P_m^* = P^*/0.3 . \quad (46)$$

Table 2. *Effects of duration of wing rotation on lift and power (α_m adjusted for balanced hovering flight)*

$\Delta\tau_r/\tau_c$	α_m (degrees)	$\overline{C_L}$	$C_{W,t}^+$	$C_{W,t}^-$	$C_{W,r}^+$	$C_{W,r}^-$	C_W
0.36	35	1.15	15.96	–1.00	0.56	–2.30	16.52
0.24	36.5	1.15	12.70	–0.66	0.26	–1.76	12.96
0.19	36.5	1.15	12.08	–0.88	0.98	–1.42	13.06

$\overline{C_L}$, mean lift coefficient; C_W, coefficient of work per cycle; $C_{W,t}^+$ and $C_{W,t}^-$, coefficients of positive and negative work for translation, respectively; $C_{W,r}^+$ and $C_{W,r}^-$, coefficients of positive and negative work for rotation, respectively; α_m, midstroke angle of attack; $\Delta\tau_r$, non-dimensional duration of wing rotation; τ_c, non-dimensional period of one flapping cycle.

The muscle efficiency, η, is:

$$\eta = P^*/R_m\,, \tag{47}$$

where R_m is the body-mass-specific metabolic rate. Lehmann et al. (2000) measured the body-mass-specific CO_2 released for several species of fruit fly in the genus *Drosophila*. For *D. virilis* in hovering flight, the rate of CO_2 release was $30.1\,ml\,g^{-1}\,h^{-1}$, corresponding to a body-mass-specific metabolic rate of $170\,W\,kg^{-1}$. The calculated muscle-mass-specific power and muscle efficiency are $P_m^*=95.7\,W\,kg^{-1}$ and $\eta=17\,\%$.

It is very interesting to look at the drag on the wing. In the above case ($\Delta\tau_r=0.24\tau_c$, $\alpha_m=36.5\,°$), the mean drag coefficient $\overline{C_D}$ over an up- or downstroke is 1.46; $\overline{C_L}/\overline{C_D}=1.15/1/46=0.79$. We see that, for this tiny hovering insect, its wings must overcome a drag that is 27 % larger than its weight to produce a lift that equals its weight. (This is very different from a large fast-flying bird, which only needs to overcome a drag that is a small fraction of its weight, and from a hovering helicopter, the blades of which need to overcome a drag that represents an even smaller fraction of its weight.)

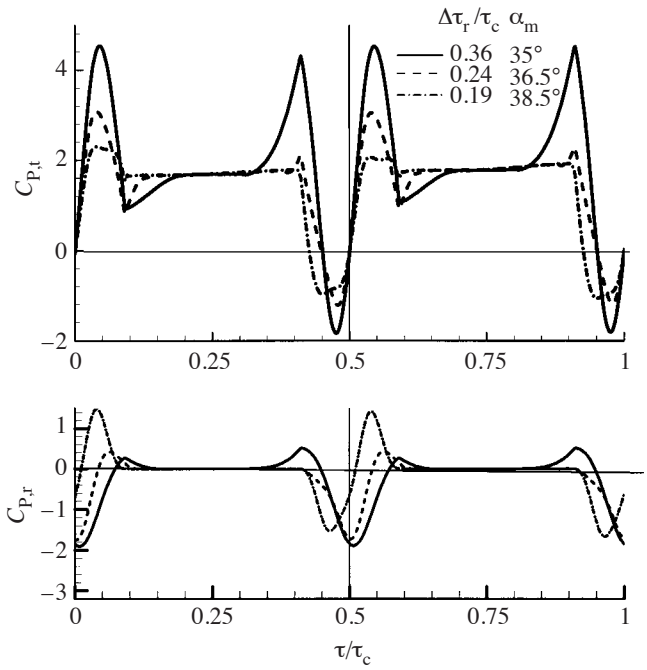

Fig. 14. The power coefficients for translation ($C_{P,t}$) and rotation ($C_{P,r}$) *versus* time during one cycle for three different values of the non-dimensional duration of wing rotation $\Delta\tau_r$. Symmetrical rotation; midstroke angle of attack α_m was adjusted to make the mean lift equal to insect weight. τ_c, non-dimensional period of one flapping cycle; τ, non-dimensional time.

Comparison between the calculated results and previous data

The above results showed that, for a duration of wing rotation $\Delta\tau_r=0.19\tau_c$ and $\Delta\tau_r=0.24\tau_c$, the power expenditure for hovering flight in *Drosophila virilis* was relatively small compared with that for larger values of $\Delta\tau_r$. The corresponding non-dimensional mean rotational velocities are approximately 1 (maximum $\dot{\alpha}^+$ is approximately 2, as seen in Fig. 13A). This mean rotational velocity is close to the value of 0.95 measured in the free forward flight of *Drosophila melanogaster* [data in Table 4 of Ennos (1989) multiplied by $R/r_2=1/0.58$ because a different reference velocity was used]. It is also close to that measured in free hovering flight in craneflies, hoverflies and droneflies: approximately 0.9, 1.2 and 0.9, respectively [data in Table 2 of Ellington (1984a) multiplied by 1/0.58]. Therefore, both from measurements from similar insects and from the calculated efficiency, it is reasonable to assume a $\Delta\tau_r$ of approximately 20 % of τ_c.

The calculated midstroke angle of attack α_m is approximately 37 ° (see Table 2; $\alpha_m=36.5\,°$ and $\alpha_m=38.5\,°$ for $\Delta\tau_r=0.24\tau_c$ and $\Delta\tau_r=0.19\tau_c$, respectively). Vogel (1967) measured the angle of attack for tethered *Drosophila virilis* flying in still air; α_m was approximately 45 °. Our calculated value is smaller than this value, which is reasonable since the calculated value is for free and balanced flight whereas the measured value was for tethered flight in which the insect could use a larger angle of attack. Ellington (1984a) observed many small insects in hovering flight, including the fruit fly, and found that the angle of attack employed was approximately 35 °. The predicted value thus is in good agreement with observations.

The calculated body-mass-specific power P^* and muscle efficiency η were $28.7\,W\,kg^{-1}$ and 17 %, respectively. Lehmann and Dickinson (1997) studied the muscle efficiency of the fruit fly *Drosophila melanogaster* by simultaneously measuring the metabolic rate and the flight kinematics. Using the measured stroke amplitude and frequency, they estimated the mean specific power using a quasi-steady aerodynamics

method. Their estimate of P^* for hovering flight was $17.9\,W\,kg^{-1}$, only approximately half the value calculated using the present unsteady flow simulation method. Their measured metabolic rate was approximately $199\,W\,kg^{-1}$. As a result, they obtained a muscle efficiency of approximately 9 %, approximately half that obtained in the present study. In their recent work on unsteady force measurements on a model fruit fly wing, Sane and Dickinson (2001) showed that the drag on the wing was much larger than the quasi-steady estimate of Lehmann and Dickinson (1997). On the basis of the measured drag, they suggested that the previous value of muscle efficiency presented by Lehmann and Dickinson (1997) should be adjusted to approximately 20 %. This is similar to the value calculated in the present study.

The calculated results show that, for the advanced rotation and delayed rotation cases, the energy expended for a given mean lift is much larger than that in the case of symmetrical rotation. On the basis of these results, symmetrical rotation should be employed by the insect for balanced, long-duration flight and advanced rotation and delayed rotation should be employed for manoeuvring. This agrees with observations on balanced flight (Ennos, 1989) and manoeuvring (Dickinson et al., 1993) in the fruit fly *Drosophila melanogaster*.

List of symbols

c	mean chord length
C_D	drag coefficient
$\overline{C_D}$	mean drag coefficient (over an up- or downstroke)
C_L	lift coefficient
$\overline{C_L}$	mean lift coefficient
$\bar{C}_{L,w}$	mean lift coefficient for supporting the insect's weight
C_P	power coefficient
$C_{P,a}$	coefficient of aerodynamic power
$C_{P,i}$	coefficient of inertial power
$C_{P,r}$	coefficient of power for rotation
$C_{P,t}$	coefficient of power for translation
$C_{Q,a,r}$	coefficient of aerodynamic torque for rotation
$C_{Q,a,t}$	coefficient of aerodynamic torque for translation
$C_{Q,i,r}$	coefficient of inertial torque for rotation
$C_{Q,i,t}$	coefficient of inertial torque for translation
C_W	coefficient of work per cycle
$C_{W,r}^+$	coefficient of positive work for rotation
$C_{W,r}^-$	coefficient of negative work for rotation
$C_{W,t}^+$	coefficient of positive work for translation
$C_{W,t}^-$	coefficient of negative work for translation
D	drag
dm_w	mass element of the wing
$\mathbf{F}$	aerodynamic force per unit wing area
f_x, f_y, f_z	x, y and z components of $\mathbf{F}$, respectively
$\mathbf{H}$	angular momentum of a wing
$\mathbf{i}, \mathbf{j}, \mathbf{k}$	unit vectors in the x, y and z directions, respectively
I_{xx}, I_{yy}, I_{zz}	moments of inertia of the wing about the x, y and z axes, respectively
$I_{xy}, I_{yz},, I_{xz}$	products of inertia of the wing
L	lift
m	mass of the insect
m_w	wing mass of the insect
$\mathbf{M_a}$	aerodynamic moment
$\mathbf{M_i}$	inertial moment
m_i^x, m_i^y, m_i^z	x, y and z components of $\mathbf{M_i}$, respectively
n	wingbeat frequency
O, o	origins of the inertial and non-inertial frames of reference, repectively
p	non-dimensional fluid pressure
P	mechanical power
P_a	aerodynamic power
P_i	inertial power
P^*	body-mass-specific power
P_m^*	muscle-mass-specific power
$Q_{a,r}$	aerodynamic torque for rotation
$Q_{a,t}$	aerodynamic torque for translation
$Q_{i,r}$	inertial torque for rotation
$Q_{i,t}$	inertial torque for translation
r	radial position along wing length
r_2	radius of the second moment of wing area
$\mathbf{r}$	vector distance between point o and an element on the wing
R	wing length
Re	Reynolds number
R_m	body-mass-specific metabolic rate
S	area of one wing
S_t	area of a wing pair
t	time
u, v, w	three components of non-dimensional fluid velocity
u_t	translational velocity of the wing
u_t^+	non-dimensional translational velocity of the wing
U	reference velocity (u_t averaged over a stroke)
U_m	midstroke translational velocity of a wing (or maximum of u_t)
U_m^+	maximum of u_t^+
X, Y, Z	coordinates in the inertial frame of reference
x, y, z	coordinates in the non-inertial frame of reference
α	angle of attack
α_m	midstroke angle of attack
$\dot{\alpha}$	angular velocity of pitching rotation
$\dot{\alpha}^+$	non-dimensional angular velocity of pitching rotation
$\dot{\alpha}_0^+$	a constant
$\ddot{\alpha}$	angular acceleration of pitching rotation
$\ddot{\alpha}^+$	non-dimensional angular acceleration of pitching rotation
$\Delta\tau_t$	duration of deceleration/acceleration around stroke reversal (non-dimensional)

$\Delta\tau_r$	duration of wing rotation or flip duration (non-dimensional)
η	muscle efficiency
ν	kinematic viscosity
ϕ	azimuthal or positional angle
Φ	stroke amplitude
$\dot{\phi}$	angular velocity of azimuthal rotation
$\dot{\phi}^+$	non-dimensional angular velocity of azimuthal rotation
$\ddot{\phi}$	angular acceleration of azimuthal rotation
$\ddot{\phi}^+$	non-dimensional angular acceleration of azimuthal rotation
ρ	density of fluid
τ	non-dimensional time
τ_c	period of one flapping cycle (non-dimensional)
τ_l	time when translational deceleration starts (non-dimensional)
τ_r	time when pitching rotation starts (non-dimensional)
τ_t	time when stroke reversal starts (non-dimensional)
τ_s	period of one stroke (non-dimensional)
τ_0	time when a stroke starts (non-dimensional)
$\boldsymbol{\Omega}$	total angular velocity vector of the wing

We would like to thank the two referees for their helpful comments on this manuscript. This research was supported by the National Natural Science Foundation of China.

References

Birch, J. M. and Dickinson, M. H. (2001). Spanwise flow and the attachment of the leading-edge vortex on insect wings. *Nature* **412**, 729–733.

Dickinson, M. H. and Götz, K. G. (1993). Unsteady aerodynamic performance of model wings at low Reynolds numbers. *J. Exp. Biol.* **174**, 45–64.

Dickinson, M. H., Lehman, F. O. and Götz, K. G. (1993). The active control of wing rotation by *Drosophila*. *J. Exp. Biol.* **182**, 173–189.

Dickinson, M. H., Lehman, F. O. and Sane, S. P. (1999). Wing rotation and the aerodynamic basis of insect flight. *Science* **284**, 1954–1960.

Ellington, C. P. (1984a). The aerodynamics of hovering insect flight. III. Kinematics. *Phil. Trans. R. Soc. Lond. B* **305**, 41–78.

Ellington, C. P. (1984b). The aerodynamics of hovering insect flight. IV. Aerodynamic mechanisms. *Phil. Trans. R. Soc. Lond. B* **305**, 79–113.

Ellington, C. P. (1984c). The aerodynamics of hovering insect flight. VI. Lift and power requirements. *Phil. Trans. R. Soc. Lond. B* **305**, 145–181.

Ellington, C. P., van den Berg, C. and Willmott, A. P. (1996). Leading edge vortices in insect flight. *Nature* **384**, 626–630.

Ennos, A. R. (1989). The kinematics and aerodynamics of the free flight of some Diptera. *J. Exp. Biol.* **142**, 49–85.

Hilgenstock, A. (1988). A fast method for the elliptic generation of three dimensional grid with full boundary control. In *Numerical Grid Generation in CFM'88* (ed. S. Sengupta, J. Hauser, P. R. Eiseman and J. F. Thompson), pp. 137–146. Swansea UK: Pineridge Press Ltd.

Lan, S. L. and Sun, M. (2001a). Aerodynamic of properties of a wing performing unsteady rotational motions at low Reynolds number. *Acta Mech.* **149**, 135–147.

Lan, S. L. and Sun, M. (2001b). Aerodynamic interaction between two airfoils in unsteady motions. *Acta Mech.* **150**, 39–51.

Lehmann, F.-O. and Dickinson, H. D. (1997). The changes in power requirements and muscle efficiency during elevated force production in the fruit fly *Drosophila melanogaster*. *J. Exp. Biol.* **200**, 1133–1143.

Lehmann, F.-O., Dickinson, M. H. and Staunton, J. (2000). The scaling of carbon dioxide release and respiratory water loss in flying fruit flies (*Drosophila* spp.). *J. Exp. Biol.* **203**, 1613–1624.

Rogers, S. E. and Kwak, D. (1990). Upwind differencing scheme for the time-accurate incompressible Navier–Stokes equations. *AIAA J.* **28**, 253–262.

Rogers, S. E., Kwak, D. and Kiris, C. (1991). Numerical solution of the incompressible Navier–Stokes equations for steady-state and dependent problems. *AIAA J.* **29**, 603–610.

Sane, S. P. and Dickinson, M. H. (2001). The control of flight force by a flapping wing: lift and drag production. *J. Exp. Biol.* **204**, 2607–2626.

Sun, M. and Tang, J. (2002). Unsteady aerodynamic force generation by a model fruit fly wing in flapping motion. *J. Exp. Biol.* **205**, 55–70.

Vogel, S. (1966). Flight in *Drosophila*. I. Flight performance of tethered flies. *J. Exp. Biol.* **44**, 567–578.

Vogel, S. (1967). Flight in *Drosophila*. II. Variations in stroke parameters and wing contour. *J. Exp. Biol.* **46**, 383–392.

Weis-Fogh, T. (1972). Energetics of hovering flight in hummingbirds and in *Drosophila*. *J. Exp. Biol.* **56**, 79–104.

Weis-Fogh, T. (1973). Quick estimates of flight fitness in hovering animals, including novel mechanism for lift production. *J. Exp. Biol.* **59**, 169–230.